Appl. Phys. B 87, 373–378 (2007)
DOI: 10.1007/s00340-007-2607-9

Applied Physics B
Lasers and Optics

C. BELLECCI[1,2]
M. FRANCUCCI[1]
P. GAUDIO[1,✉]
M. GELFUSA[1]
S. MARTELLUCCI[1]
M. RICHETTA[1]
T. LO FEUDO[2]

Application of a CO_2 dial system for infrared detection of forest fire and reduction of false alarm

[1] Faculty of Engineering, University of Rome "Tor Vergata", Via del Politecnico 1, 00133 Roma, Italy
[2] CRATI S.c.r.l c/o University of Calabria, 87036 Arcavata di Rende (CS), Italy

Received: 24 July 2006/Revised version: 10 January 2007
Published online: 28 March 2007 • © Springer-Verlag 2007

ABSTRACT Forest fires can be the cause of serious environmental and economic damages. For this reason considerable effort has been directed toward forest protection and fire fighting.

The means traditionally used for early fire detection mainly consist in human observers dispersed over forest regions. A significant improvement in early warning capabilities could be obtained by using automatic detection apparatus.

In order to early detect small forest fires and minimize false alarms, the use of a lidar system and dial technique will be considered.

A first evaluation of the lowest detectable concentration will be estimated by numerical simulation. The theoretical model will also be used to get the capability of the dial system to control wooded areas. Fixing the burning rate for several fuels, the maximum range of detection will be evaluated. Finally results of simulations will be reported.

PACS 42.68.Wt; 89.60.Ec; 92.60.Mt; 92.60.Iq

1 Introduction

Lidar and dial techniques are by now very well established technologies to explore atmosphere [1]. They are often used to acquire information to create or validate several models relevant to different topics of atmospheric physics, but they can also be employed in environmental monitoring of particulate and gas.

In the dial technique the lidar transmitter emits light pulses at two closely adjacent wavelengths λ_{ON} and λ_{OFF} into the atmosphere. λ_{ON} denotes the on-line wavelength where the trace gas absorption causes an additional attenuation of the radiation during passage through the atmosphere, λ_{OFF} is the associated non-absorbing off-line wavelength. The comparison of the backscattered radiation at both wavelengths yields the trace gas number density as a function of distance along field-of-view of the receiving telescope [2].

Experimental and theoretical investigations by Andreucci and Arbolino [3], Lavrov and Vilar [4, 6], Pershin et al. [5] and Utkin et al. [7, 8] have shown that lidar is a powerful tool to detect the tenuous smoke plumes produced by forest fires at an early stage of development and present considerable advantages for early forest fire detection in comparison with passive methods of fire surveillance. Full automation of the detection process requires prompt identification of the peaks corresponding to smoke plumes in the lidar return signals, but these signals may often present other peaks, resulting from various causes, among which a relevant one is the returning signal due to the long nitrogen tail of the laser pulse [9].

In previous work the authors presented the realization, use and characterization of a laser-induced sealed plasma shutter to clip off this nitrogen tail of the TE-CO_2 laser [10, 11].

The aim of this work is to underline the role of a CO_2 laser based apparatus in revealing forest fire and minimizing false alarm events. For this purpose, we propose to use our system in lidar and dial measurements configuration. The first lidar measurement is executed to evaluate the variation of the aerosol amount into the atmosphere by means of a non-absorption water wavelength. If the returned signal reports a backscattering peak, the presence of a fire will be probable. To confirm this hypothesis, a second dial measurement is needed to establish the presence of another component emitted by combustion process, as water vapor, which is largely produced at the first combustion stage. This should be done by sending a second laser pulse at a water absorbed wavelength. If also in this case an increment with respect to the standard concentration level is revealed, a second fire warning is obtained. In this way, our system is able to early detect forest fire events and, at the same time, to reduce the occurrences of false alarms since it operates with two combined and independent procedures described before.

2 System description

The lidar system is based on a home-made TEA CO_2 source in SFUR configuration [12, 13]. It permits to operate with a TEM_{00} mode and then a Gaussian pulse shape. The laser is tuneable over about 60 laser lines in the spectral range between 9–11 μm. These range compared to the visible and UV region is in good agreement with the eye-safe conditions that is required when one laser pulse is sent in free atmosphere.

The energy output is equal to 500 mJ with a giant pulse width of about 100 ns. As it is well known, this pulse is consti-

✉ Fax: +39 067259 7207, E-mail: gaudio@ing.uniroma2.it

tuted by a main peak followed a long nitrogen tail. In our set up we clipped the tail by means of a plasma-shutter.

This apparatus is well described in previous works [10, 11].

The results obtained with this device are reported in Figs. 1 and 2. The first one shows the unclipped signal, while the second, the clipped one.

We developed a rapidly tuning diffraction grating that assures a misalignment less than 0.1 mrad and a laser tuning time less than 500 ms. As investigated in previous works [14], a random error "δ" in alignment is determined sending "on" and "off" pulses of a single laser. In the case of coaxial lidar configuration, random alignment error gives an absolute error in concentration measurement. If the case of water vapour measurements with $\delta \sim 0.1$ mrad, the numerical result gives an absolute error in concentration measurement of about 100 ppm [14, 15].

The telescope is based on Newtonian configuration. The primary mirror has a diameter of 400 mm and a focal length of 2400 mm.

The photodetector is a nitrogen-cooled HgCdTe device. The data control and acquisition system is illustrated schematically in Fig. 3.

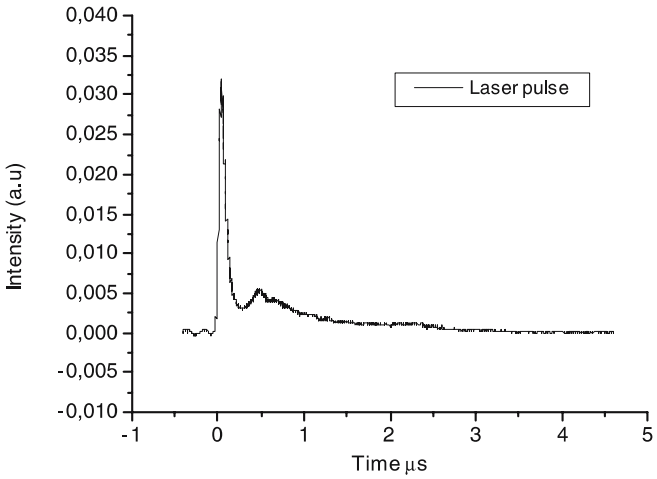

FIGURE 1 Unclipped laser pulse. Temporal profile

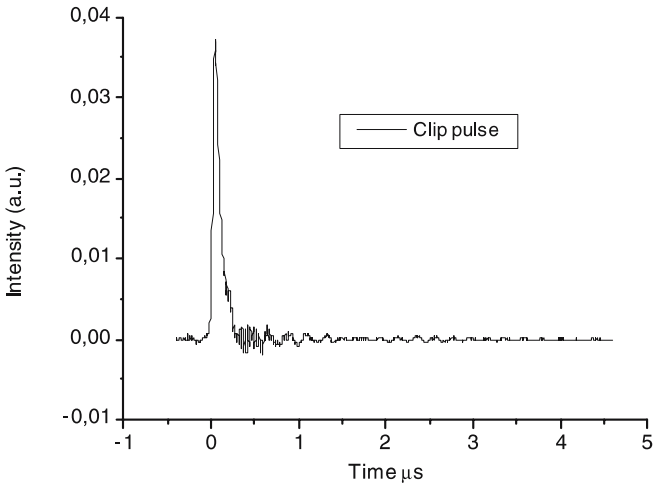

FIGURE 2 Temporal profile of truncated CO_2 laser pulse

Transmitter TEA CO_2 laser		
	Output energy	500 mJ
	Peak power	1 MW
	Pulse width	GSWP : 100 ns; tail:≈ 4 μs
	Beam divergence	0.77 mrad
	Spectral range	9–11 μm
Receiver		
	Primary ROC	2400 mm
	Primary diameter	400 mm
	ZnSe lens focal length	50 mm
	Total focal length	576.6 mm
	F.O.V.	0.88 mrad
	Detector type	HgCdTe
	Detector sensitivity	D^* 3.38 (1010 cm $Hz^{1/2}$/W)
	Detector size	1 mm^2
Acquisition system		
	Lecroy 9350 C	11 bit 1–1 G sample/s

TABLE 1 Set up parameters

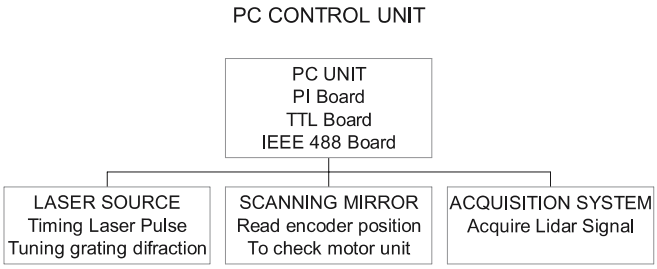

FIGURE 3 PC control system scheme

The acquisition system is based on a oscilloscope digitiser Lecroy 9350 C model with a 500 MHz band width, with vertical resolution up to 11 bits of. All the system is checked by a computer. Into the PC are inserted a compatible IEEE 488 and 16 channel optical isolated I/O TTL boards. The first board using a GPIB bus transfer the backscattered data in the PC memory, the second give TTL pulse for timing the laser shot and move the two scanning mirror motors. The same board reads the TTL input from scanner module encoder to known the exact position where we send the laser radiation. At the end there is another Physics Instruments board to move the diffraction grating. The program is based on LABVIEW software showing a simple interface between PC and the operator.

3 Theoretical overview

To evaluate the feasibility and the performances of a forest fire early detection system, a smoke diffusive model has been taken into account [16]. The ideal smoke model for this purpose would consider a large number of variables and parameters concerning the combustion process, vegetation typology, ground morphology and climate.

We choose a simplified model, and implemented it to obtain realistic results together with a computational effort as low as possible. This model includes such aspects that are explicitly correlated to the infra-red and optical properties of the smoke plume and it has been developed in the steady state and unsteady state cases.

The smoke plume model has been subsequently coupled to a dial sensitivity analysis, in order to estimate the system efficiency.

3.1 *Smoke diffusive model*

The simplified smoke model is based on three main variables: the fuel combustion rate M, expressed in kg/min; the amount of air involved into the combustion of one kilogram of vegetal fuel (taking into account the appropriate air excess); the smoke source size R_s (the radius of the ideal circumference containing the burning fuel at altitude zero).

The reference fuel has been defined by Johnson [17] on the basis of the following percentage mass composition:

- Carbon, C = 0.505;
- Hydrogen, H = 0.06;
- Oxygen, O = 0.42;
- Ashes, A = 0.015.

The moisture fraction usually enclosed in vegetal materials varies from 15 to 80 mass percent [17]. A value of 40% has been assumed.

The combustion process is a chemical reaction during which the carbon and the hydrogen within the fuel are combined with oxygen (both the oxygen already included in the fuel composition and the oxygen from atmospheric air) and produce carbon dioxide and water. It is assumed that complete combustion of fuel occurs, so all the carbon and the hydrogen are transformed by combustion; 1 kg of the reference fuel includes:

- 400 g of H_2O equal to 22.22 moles;
- 303 g of C equal to 25.25 moles;
- 36 g of H equal to 36.00 moles;
- 252 g of O equal to 15.75 moles.

In order to obtain complete combustion, 26.375 moles of O_2 are required in additional to the oxygen already included in the fuel.

The smoke produced by combustion becomes more and more mixed with cold atmospheric air with increasing height above the source level. It is assumed that the gas, in an elementary volume, consists of smoke for a fraction $q_s < 1$, and for the remaining fraction $q_a = 1 - q_s$, by atmospheric gases. Once the function $q_s(x, y, z)$ and the composition of the atmospheric air are known, it is possible to calculate the composition of the smoke plume.

It has been also assumed that the concentration of the combustion products, q_s, is maximum and equal to 1 at altitude zero and time zero.

The smoke diffusion process is governed by the continuity equation:

$$\operatorname{div}(q_s \bar{v}) = \frac{\partial q_s}{\partial t}\,, \tag{1}$$

where $\bar{v}$ represents the velocity field which components are the diffusion rate, the mean wind velocity (horizontal component only) and the buoyancy rate (in the vertical direction only) [16].

This kind of problem must be resolved through the simultaneous computation of the q_s function values over a 3D grid. If the vertical diffusion velocity component is neglected, the problem becomes two-dimensional; thus, the continuity equation is much more simple to handle for numerical integration.

It is assumed that the smoke volume produced by the source in the unit time, its chemical composition and its temperature are not time-dependent, so the right hand term of (1) is null. Moreover, the smoke is considered divided in infinitely thin disks. Each one is produced at a given time, moves upwards with a buoyancy rate v_b and does not interact with the smoke disk produced at different times.

It is useful to transform (1) in cylindrical coordinates:

$$\frac{K}{v_b}\frac{1}{x}\frac{\partial}{\partial x}\left(x\frac{\partial q_s}{\partial x}\right) = \frac{\partial}{\partial z}(q_s)\,, \tag{2}$$

where $K = 0.1\ \mathrm{m^2/s}$ represents the constant diffusion coefficient and $v_b = 1\ \mathrm{m/s}$ the buoyancy rate [18]. The solution of (2) can be obtained by using numerical methods [19, 20]. In this manner we studied the behavior of the combustion products into the atmosphere, considering only 1 kg of vegetal fuel burning (Fig. 4).

The most important parameter, in the early fire detection, is the time factor. Operating during the combustion developing phase allows one to limit the subsequent damages. This phase induces a situation of great instability within the instantaneous established energetic flows; moreover, the temperature raise produces an increment of the combustion rate, from 0.4 kg/min to 0.9 kg/min [21, 22].

Figures 5 and 6 describe the conformation of the smoke plume (in terms of all combustion products) at two different times, the first after 15 min and the second after 60 min.

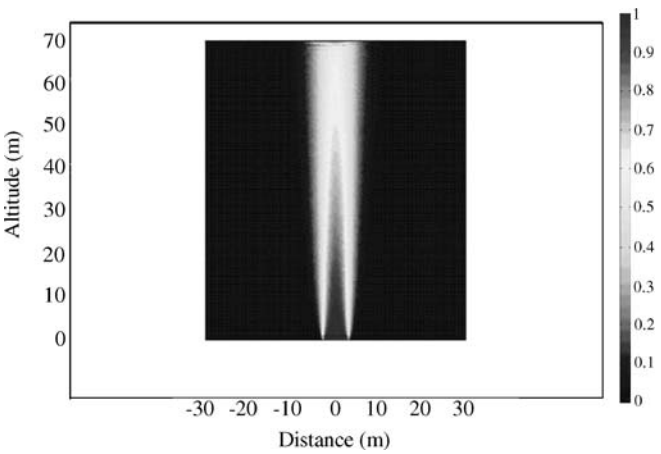

FIGURE 4 Distribution of combustion products

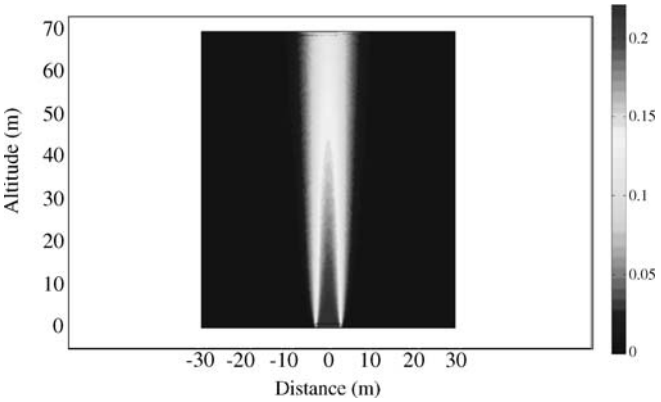

FIGURE 5 Distribution of combustion products at $t = 900$ s

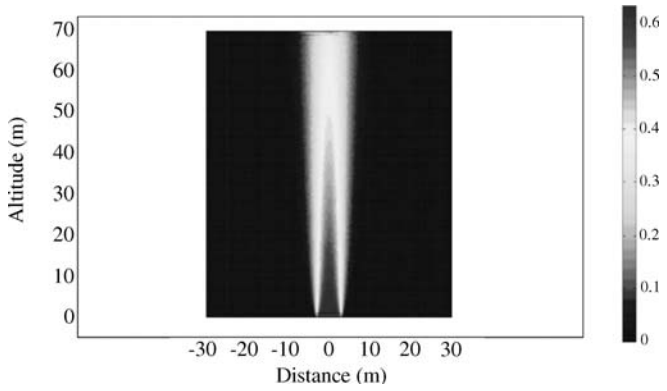

FIGURE 6 Distribution of combustion products at $t = 3600$ s

3.2 *Dial sensitivity analysis*

The basic concept of the laser remote sensing of atmospheric constituents using by dial system involves the intensity measurement of the backscattered radiation as a function of the transmitted frequency. For density profiles measurements, two laser frequencies (λ_{ON} and λ_{OFF}) are selected, such that λ_{ON} and λ_{OFF} are on-resonance and off-resonance, respectively, with an absorption transition of the molecular specie which is begin measured. The concentration of the absorbing species may be deduced from the differential absorption of the backscattered signal at λ_{ON} wavelength compared to that at λ_{OFF}.

The instantaneous power of the backscattered lidar radiation, P, may be given approximately by:

$$P(\lambda, R) = P_0 \frac{A_0}{R^2} \beta(\lambda, R) \frac{c\tau}{2} \exp\left[-2 \int_0^R k(\lambda, R')\, \mathrm{d}R'\right], \quad (3)$$

where P_0 is the output laser power, R the distance of the incoming radiation, c the speed of light, A_0 the area of primary mirror telescope, τ the temporal width of the laser pulse, β is the backscattered coefficient and k the atmospheric extinction coefficient [23].

Using (3) for the two different wavelength, one sees that it is easy to obtain the path average concentration n of the absorbing molecule, namely

$$n(R) = \frac{1}{2\,(\sigma_{on} - \sigma_{off})} \left[\frac{\mathrm{d}}{\mathrm{d}R}\left\{\ln\left[\frac{P\,(\lambda_{off}, R)}{P\,(\lambda_{on}, R)}\right] - \ln\left[\frac{\beta\,(\lambda_{on}, R)}{\beta\,(\lambda_{off}, R)}\right]\right\} + k_0\,(\lambda_{off}, R) - k_0\,(\lambda_{on}, R)\right], \quad (4)$$

where the index "on" (or "off") indicates the value referred to the absorption band (or to the detuned wavelength), P is the power received by the detector, σ the differential absorption cross-section, β the backscattered coefficient and k_0 the total atmospheric extinction exclusive of the quantity relating to the absorption due to the substance that is being studied [24].

The average minimum concentration that can be revealed by the dial system, n_{min}, can be evaluated using two different approaches depending on the considered distance R between the laser source and the target molecule [25].

For the greater values of R, the minimum concentration can be evaluated setting the difference in the return signals ΔP_r produced by the differential absorption of the absorbing species equal to the noise equivalent power (NEP) of the detector. In this case it may be shown that [25]:

$$n_{min} = \frac{(\mathrm{NEP})\pi R}{2K\varrho A P_0 (\Delta\sigma) \exp(-2\beta R)}, \quad (5)$$

where K is the receiver efficiency, ϱ is the reflectivity of the topographic target, A is the area of the receiving telescope, P_0 is the output power of the laser beam, $\exp(-2\beta R)$ is the atmospheric attenuation and $\Delta\sigma$ is the difference in the absorption coefficients of the pollutant at the two wavelengths.

At shorter ranges a more restrictive limitation may occur due to the inability of the measurement system to distinguish between the fractional change in the lidar return signal $(\Delta P_r/P_r)$ due to real variations of the species concentrations and random fluctuations caused by atmospheric turbulence and other perturbations. For this case, it was shown that

$$n_{min} = \frac{5 \times 10^3 (\Delta P_r/P_r)}{(\Delta\sigma) R}, \quad (6)$$

where the value of $(\Delta P_r/P_r)$ is a function of both, the dial system parameters and atmospheric effects.

4 Results and discussion

The early combustion phase of the vegetable matter causes a great amount of water vapor emission. Thus the water molecule behavior has been studied to obtain a fire detection system, which is ready and efficient also before the flame propagation. Measuring the water concentration peak after a revelation of the aerosol density increment (referred to the standard mean atmospheric value) represents a good method to reduce false alarms occurrence employing a dial system.

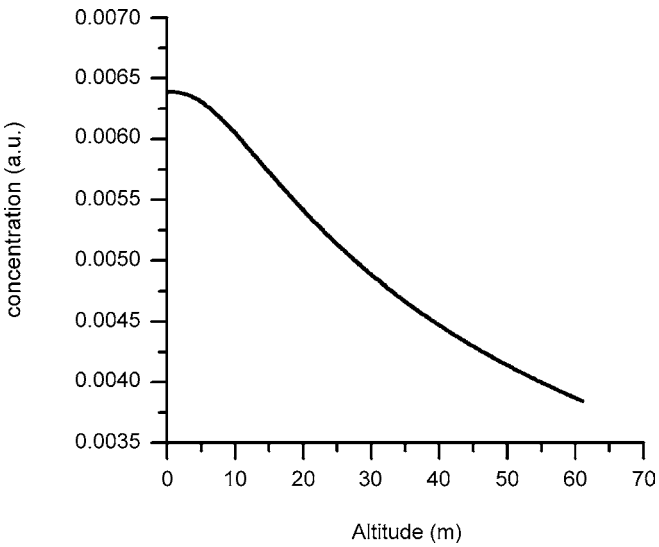

FIGURE 7 Combustion products concentration as a function of the distance x

As shown in Fig. 7, the combustion products concentration has been reported as a function of the altitude z and the distance x in the steady state case hypothesis. The first graph confirms that the 0.45% mass-fraction is present at the altitude of 40 m, assuring the presence of a sufficient water vapor concentration without reaching the system sensitivity limit. This is in agreement with the simulated lidar returned signal (Fig. 8) which reports remarkable water peaks at different lidar system–smoke plume distances at the reference altitude (30–40 m).

In order to quantify the increment in water vapor concentration, it is necessary to evaluate the light absorption of the two different wavelengths by this molecule (as seen in Sect. 3.2). The choice of these wavelengths has been made on the basis of our experimental results shown in previous works [26–28]. So the "on" and "off" lines are, respectively, $10R20$ and $10R18$ in the branch at 10 μm. The $10R20$ corresponds to 10.591 μm (944.198 cm^{-1}) and the $10R18$ to 10.571 μm (945.984 cm^{-1}). At these wavelengths the difference in the absorption coefficients of the water molecule ($\Delta\sigma$) is equal to 7.7×10^{-4} $cm^{-1}atm^{-1}$ and the value of attenuation coefficient (α) is 0.05 km^{-1} [29].

Referring to the combustion of 1 kg of vegetable matter burning in steady conditions, Fig. 9 brings out how the concentration reported by the system during a forest fire, is perfectly inside the region bordered by the two dial limit curves for a dial system–forest fire distance, which varies from 200 m to 10 km (the dial detector sensitivity is limited by the differential return ($\Delta P_r/P_r$) at short ranges and by detector noise (NEP) at the longer ranges).

As regards the unsteady state case, the simulation has been set up in order to reproduce the conditions within an hour from the ignition, in the hypothesis that the fuel burns at 0.4 kg/min. This low value has been chosen to reproduce the worse condition for the detection system; therefore if the dial system is able to early reveal a fire burning in these conditions, then it will surely succeed at greater combustion rates. Numerical computations lead to the estimated minimum time,

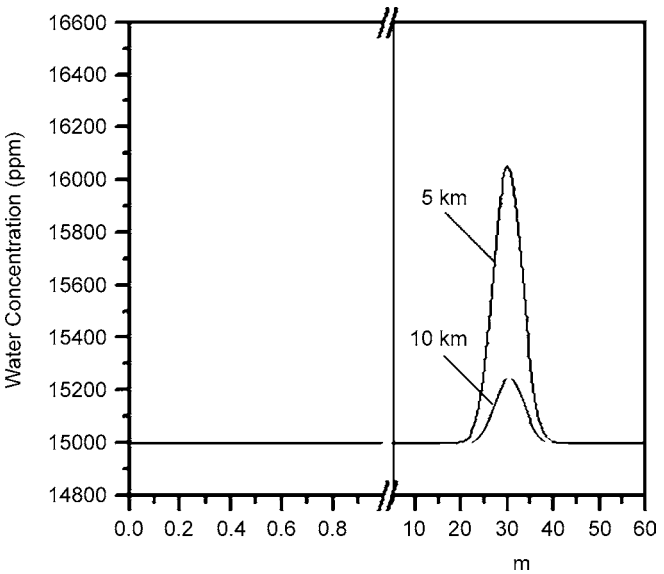

FIGURE 8 Water concentration peaks measured at 5 and 10 km

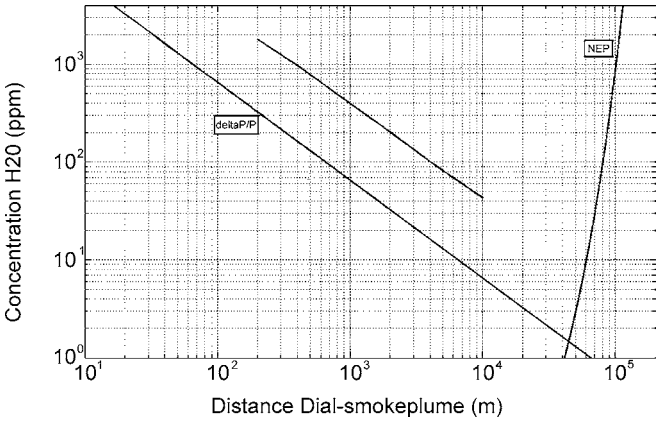

FIGURE 9 Dial system limit concentration curves in the steady-state case

elapsed since the ignition stage, to obtain a valid fire report by the dial system. The system succeeds in revealing the fire after 60 seconds from its ignition, as it can be seen from the graphs reported in Figs. 10 and 11.

In conclusion, the obtained results demonstrate that the employment of a dial system offers considerable advantages for early forest fire detection due to its higher sensitivity, ability to accurately locate the fire with very low false alarms occurrence and the high relative degree of eye safety provided by lasers operating in the infrared compared to the visible and

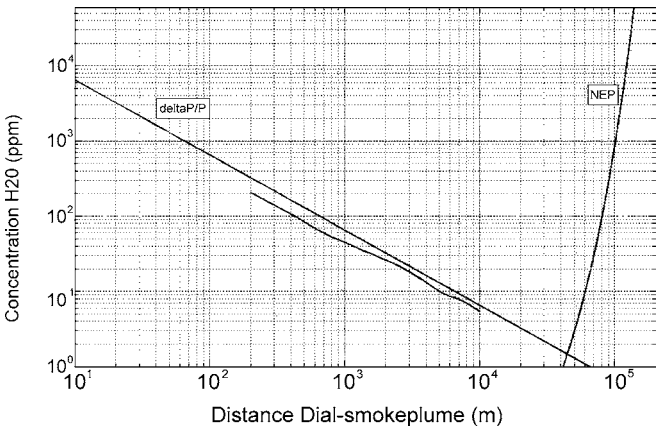

FIGURE 10 Concentration limit detectable at 48 s

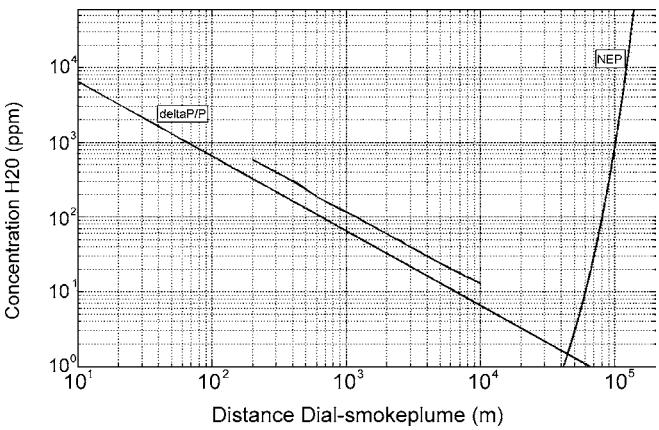

FIGURE 11 Concentration limit detectable at 60 s

UV region. These are the main prerogatives for implementing an efficient, ready and inexpensive system.

REFERENCES

1 G. Fiocco, L.D. Smullin, Nature **199**, 1275 (1963)
2 R.M. Schotland, J. Appl. Meteorol. **13**, 71 (1974)
3 F. Andreucci, M. Arbolino, Nuovo Cim. **16**, 51 (1993)
4 A. Lavrov, R. Vilar, Application of lidar at 1.54 μm for forest fire detection. Remote sensing for earth science, ocean and sea ice applications, **3868**, Bellingham, SPIE (1999), pp. 473–477
5 S. Pershin, W.M. Hao, R.A. Susott, R.E. Babbitt, A. Riebau, Estimation of emission from Idaho biomass fire using compact eye-safe diode lidar. Application of lidar to current atmospheric topics III, **3757**, Bellingham, SPIE (1999), pp. 60–6
6 R. Vilar, A. Lavrov, Appl. Phys. B **71**, 225 (2000)
7 A. Utkin, A. Fernandes, L. Costa, R. Vilar, F. Simoes, Appl. Phys. B **74**, 77 (2002)
8 A. Utkin, A. Fernandes, R. Vilar, A. Lavrov, Forest fire detection by means of lidar. Forest fire research and wildland safety, Proceedings of the IV International Conference on Forest Fire Research (Millpress, Rotterdam, 2002), p. 58
9 A. Fernandes, A. Utkin, A. Lavrov, R. Vilar, Pattern Recognition **37**, 2039 (2004)
10 C. Bellecci, I. Bellucci, P. Gaudio, S. Martellucci, G. Petrocelli, M. Richetta, Rev. Sci. Instrum. **74**, 1064 (2003)
11 C. Bellecci, P. Gaudio, S. Martellucci, E. Penco, M. Richetta, Rev. Sci. Instrum. **76**, 026 115 (2005)
12 R. Barbini, F. Colao, A. Petri, Nuovo Cim. D **13**, 143 (1991)
13 P.G. Gobbi, G.C. Reali, Opt. Commun. **52**, 195 (1984)
14 C. Bellecci, F. De Donato, Appl. Opt. **38**, 5212 (1999)
15 P. Aversa, C. Bellecci, G. Benedetti Michelangeli, G. Caputi, F. De Donato, P. Gaudio, M. Valentini, R. Zoccali, Proc. SPIE **3104**, 154 (1997)
16 F. Andreucci, M. Arbolino, Nuovo Cim. **16**, 35 (1993)
17 A.J. Johnson, *Fuel and Combustion Handbook* (McGraw-Hill, New York, 1951)
18 F.A. Gifford Jr., An outline of theories of diffusion in the lower layers of the atmosphere, *Meteorology and Atomic Energy*, ed. by D.H. Slade (U.S. Atomic Energy Commission, National Technical Information Service, U.S. Department of Commerce Springfield, 1996)
19 W.H. Press, B.P. Flannery, S.A. Teukolsky, W.T. Vetterling, *Numerical Recipes* (Cambridge University Press, New Rochelle, 1986)
20 A.W.M. van Schijndel, Building Environ. **38**, 319 (2003)
21 M.J. Spearpoint, J.G. Quintere, Combust. Flame **123**, 308 (2000)
22 F. Costa, D. Sandberg, Combust. Flame **139**, 227 (2004)
23 R.M. Measures, *Laser Remote Sensing* (Wiley, New York, 1984)
24 R. Barbini, F. Colao, L. Fiorani, A. Paolucci, Lidar atmosferico: aspetti legislativi, scientifici e tecnologici, ENEA, Centro Ricerche, Frascati, Roma
25 N. Menyuk, D.K. Killinger, E. DeFeo, Appl. Opt. **21**, 2275 (1982)
26 C. Bellecci, G. Caputi, F. De Donato, P. Gaudio, M. Valentini, Nuovo Cim. **18**, 463 (1995)
27 C. Bellecci, S. Martellucci, P. Aversa, G. Caputi, F. De Donato, P. Gaudio, M. Richetta, R. Zoccali, Romanian J. Optoelectron. **6**, 23 (1998)
28 C. Bellecci, L. Casella, S. Federico, P. Gaudio, T. Lo Feudo, S. Martellucci, M. Richetta, P. Vetrò, Evolution study of a water vapor plume using a mobile CO_2 dial system, EUROPTO European Symposium on Remote Sensing, Tolose, France, 17–21 September (2001), vol. 4539, pp. 180–190
29 W.B. Grant, J.S. Margolis, A.M. Brothers, D.M. Tratt, Appl. Opt. **26**, 3033 (1987)